Study of Solar Flares with Highest Resolution Observations

Haimin Wang
Big Bear Solar Observatory
Institute for Space Weather Sciences
New Jersey Institute of Technology

- Solar flares: Release of magnetic energy: 10^{22} — 10^{25} Joule (1 to 1000 billion atomic bombs)

Hinode/SOT

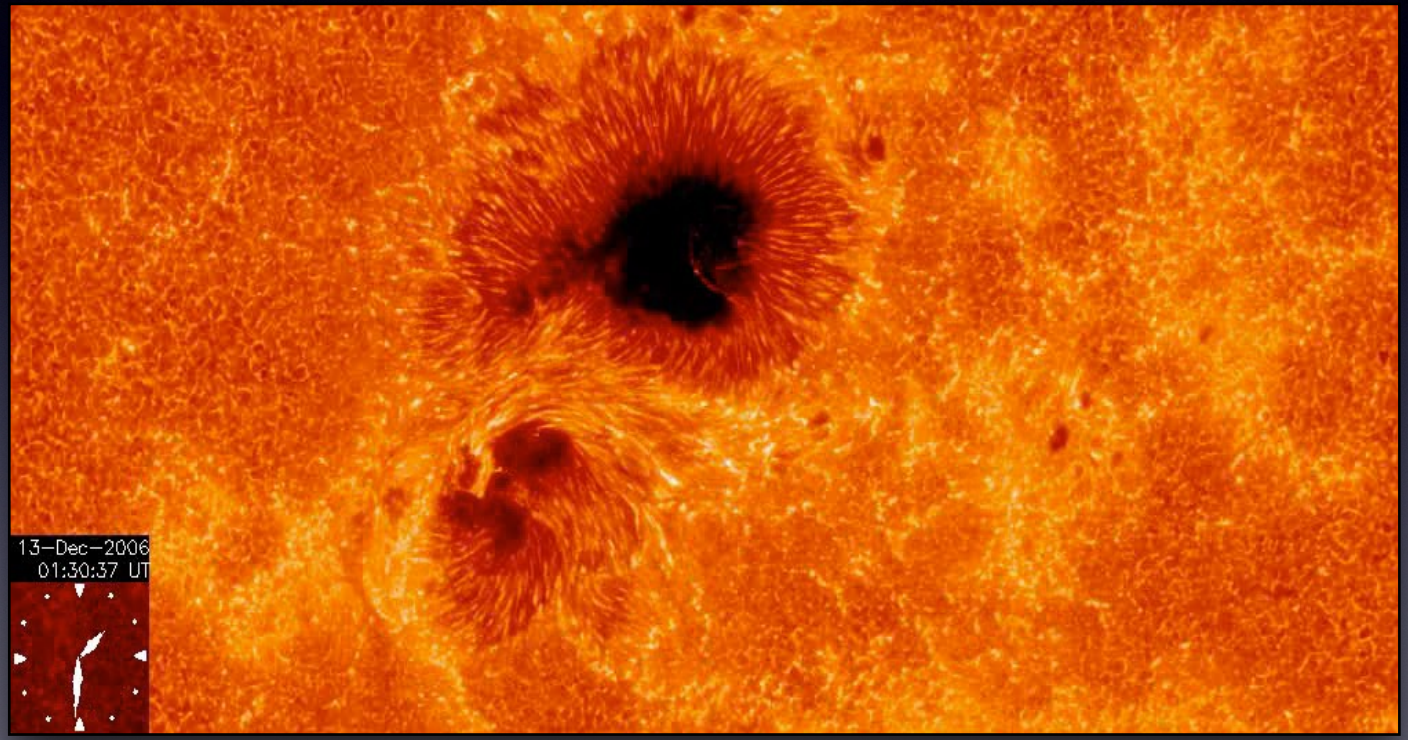

Connecting photospheric field to the activity seen in the corona

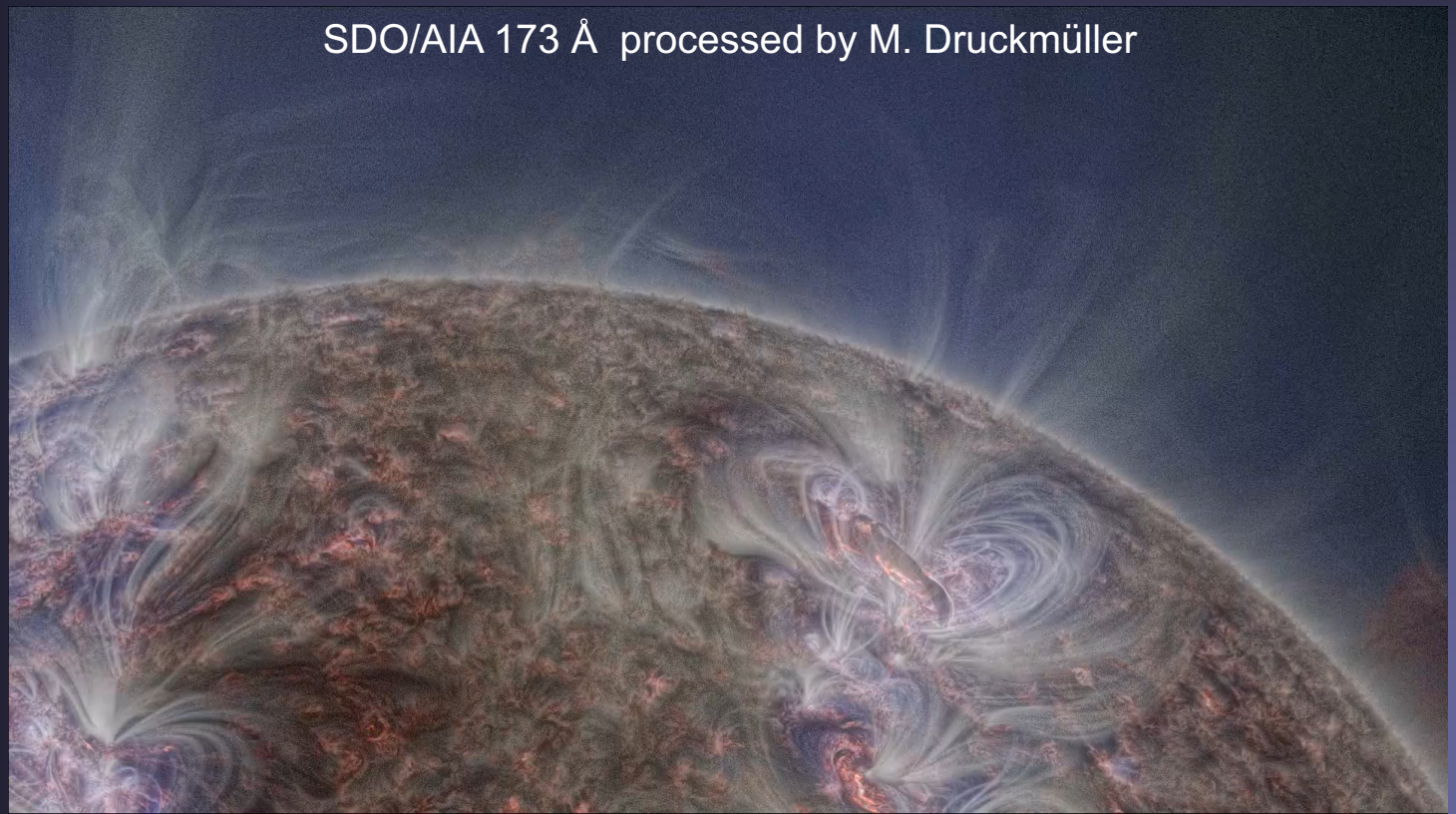

Physics of Solar Eruptions

Filament eruptions are often associated with CMEs- the eruptive filament making the core of the CME.

Two ribbon flares are due to filament or fluxropes cutting through arcade fields and reconnect at higher and higher altitudes

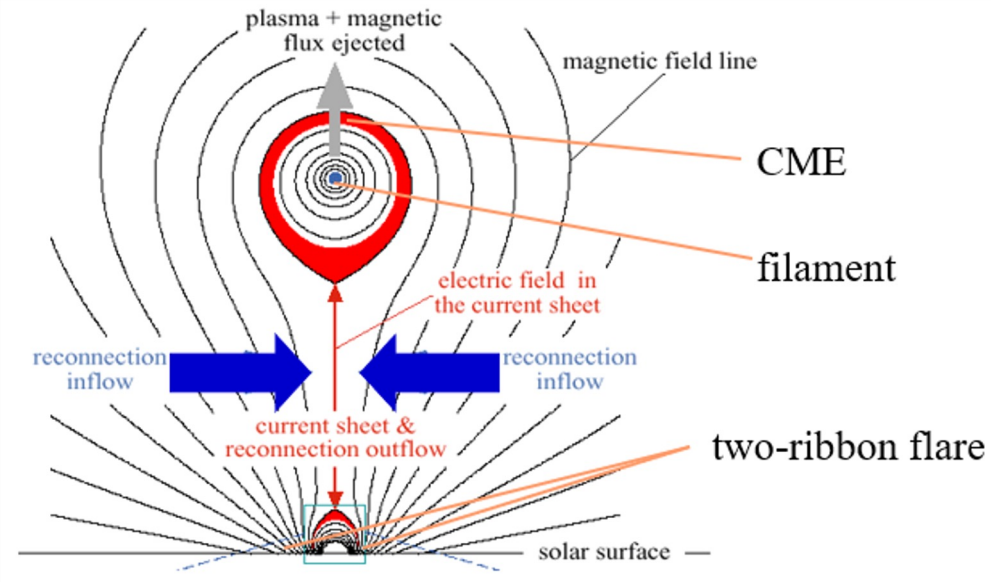

A schematic flux rope model for filament/CME and flare

Lin et al. (2004)

Flares are key sources of Space Weather Effects

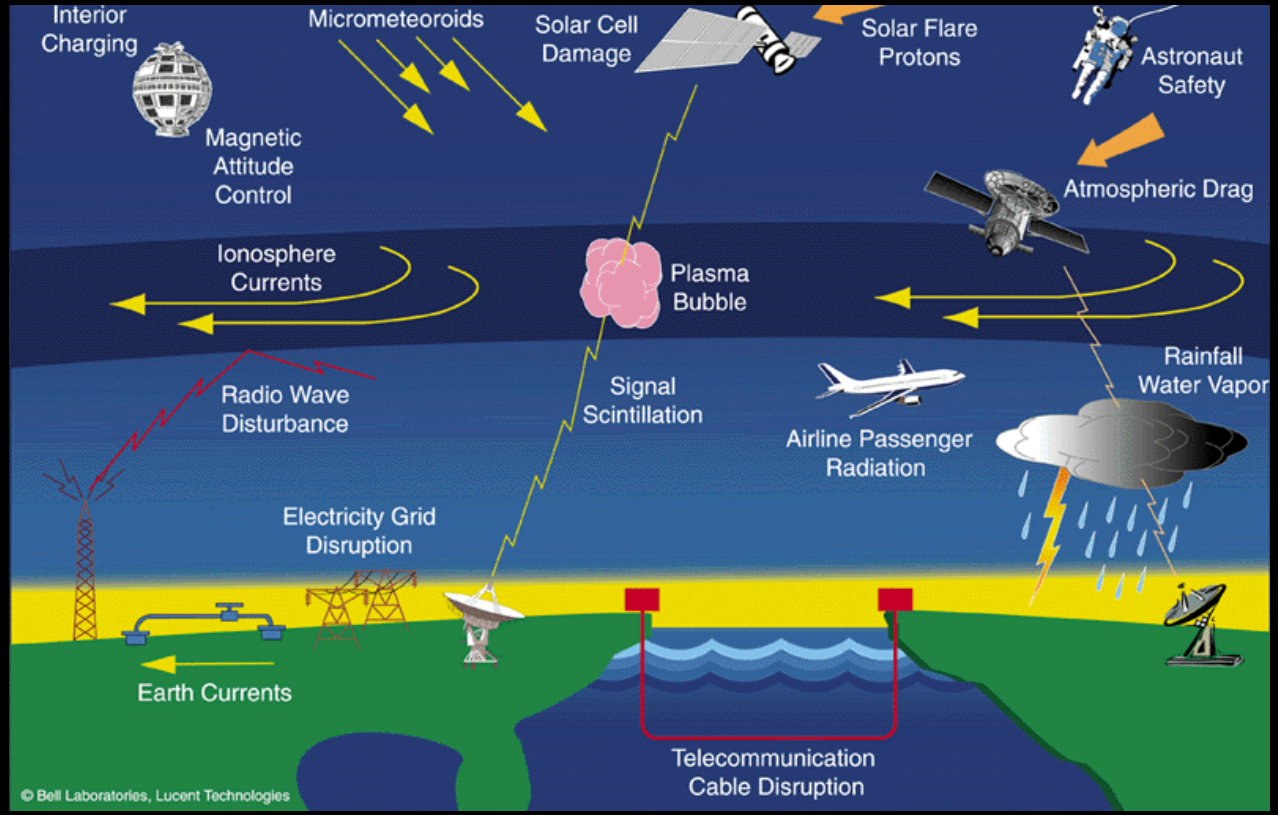

Image: L.Lanzerotti, Lucent Bell Labs

Basic Question:

In highest resolution and cadence, what solar flares would look like? What kind of dynamics can we see in flaring solar active regions (0.05” resolution, Field of view is limited to 100”)

Fine structure of eruption of magnetic ropes

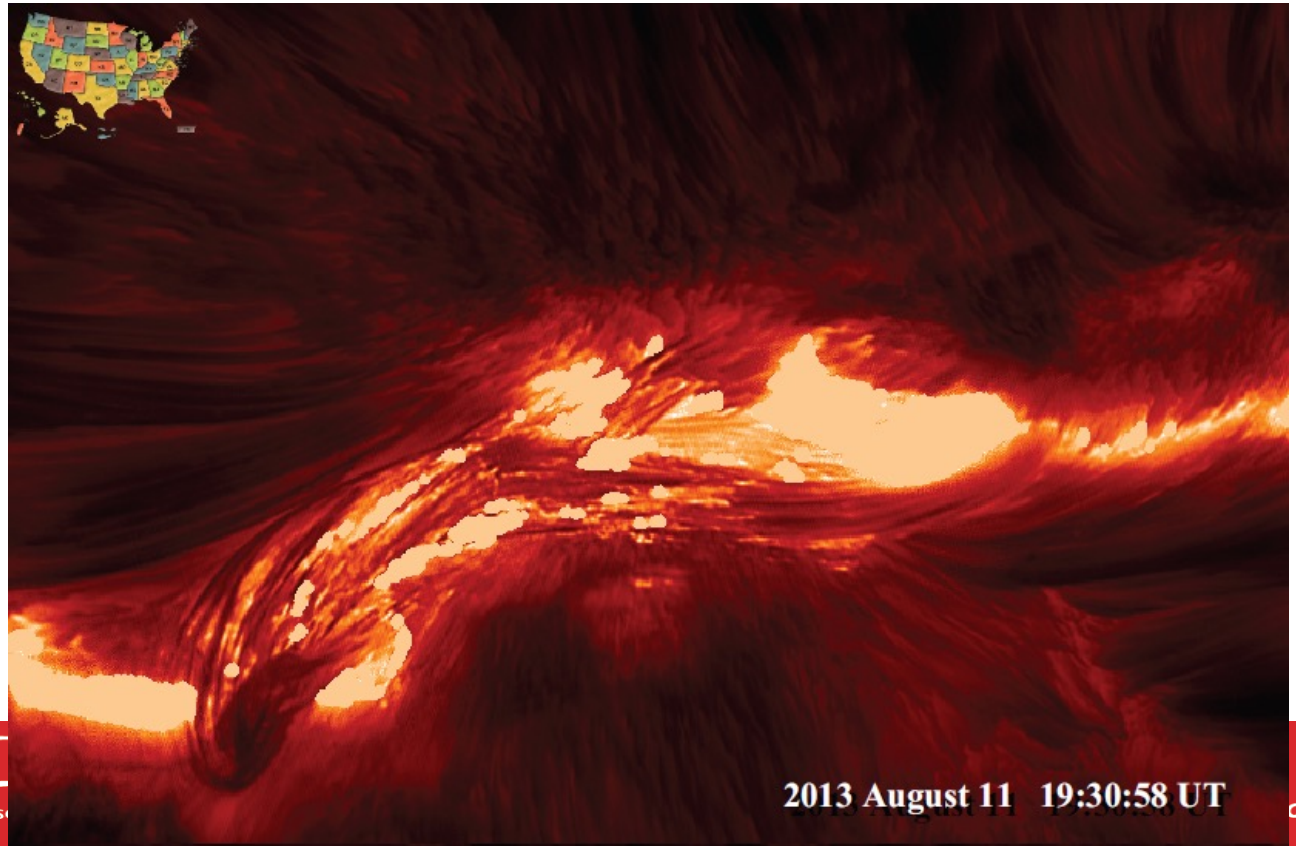

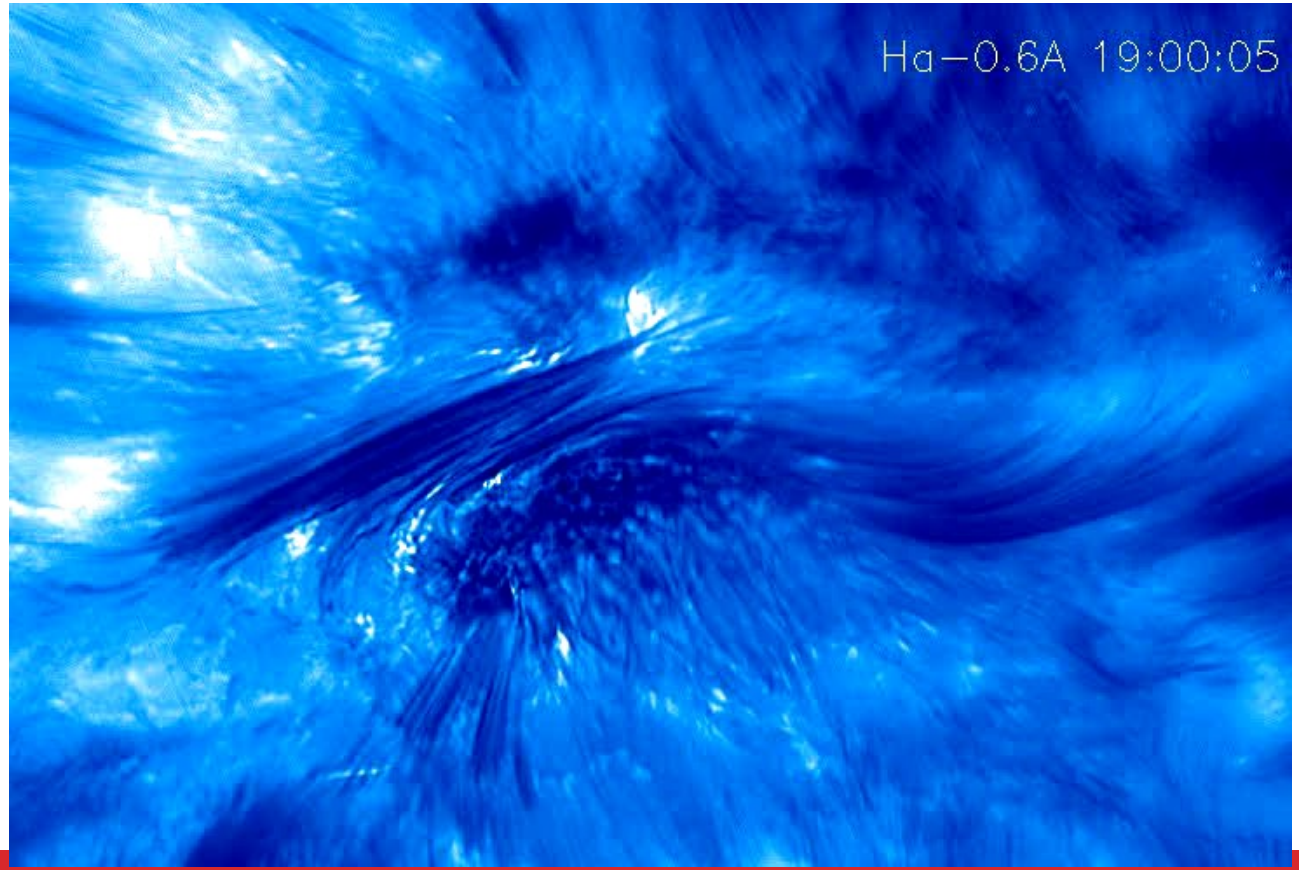
Ha−0.6A 19:00:05

GST Observations of an Active FR on 2013 August 11

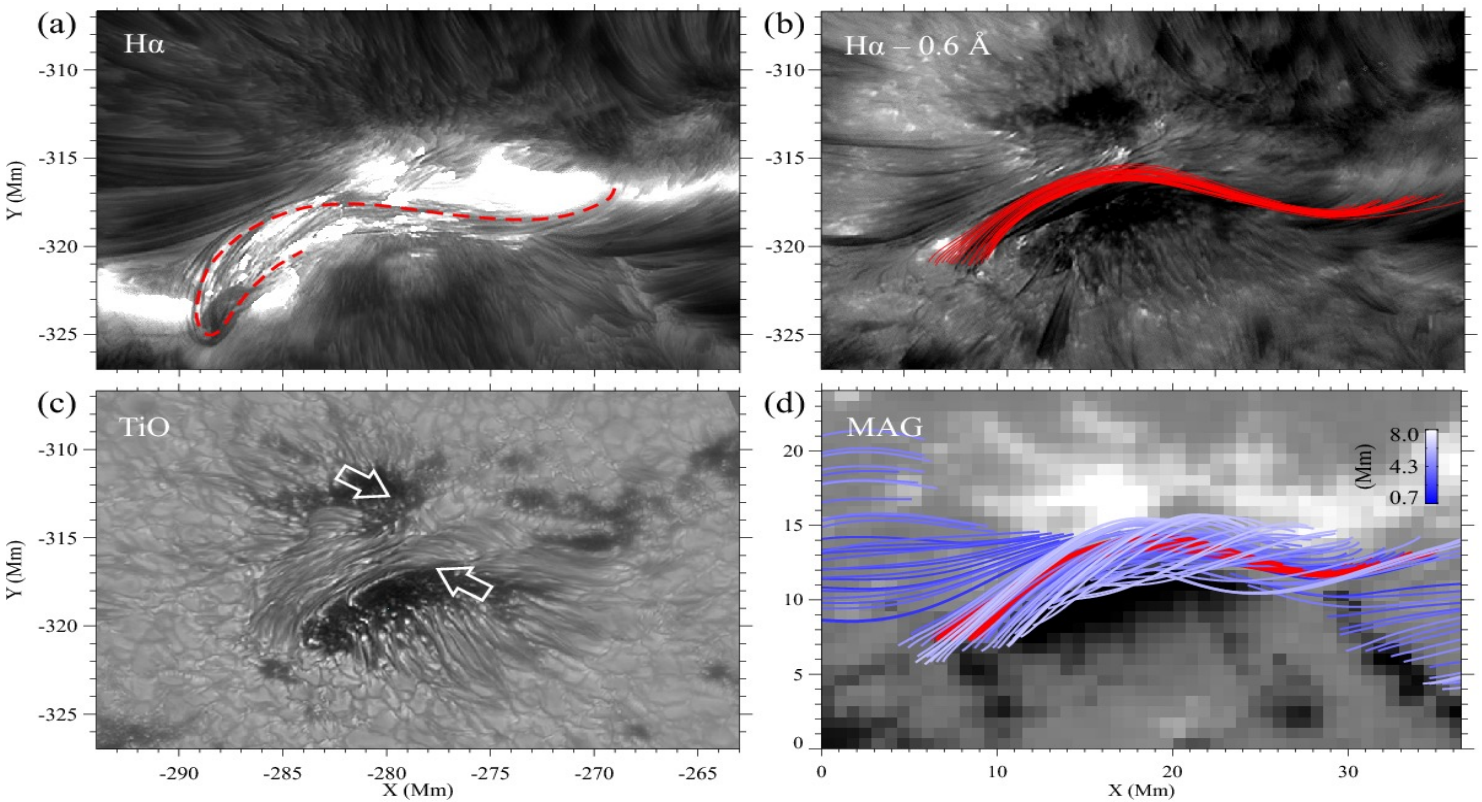

Wang et al. (2015) Nature Communications

NIRIS Magnetogram movie

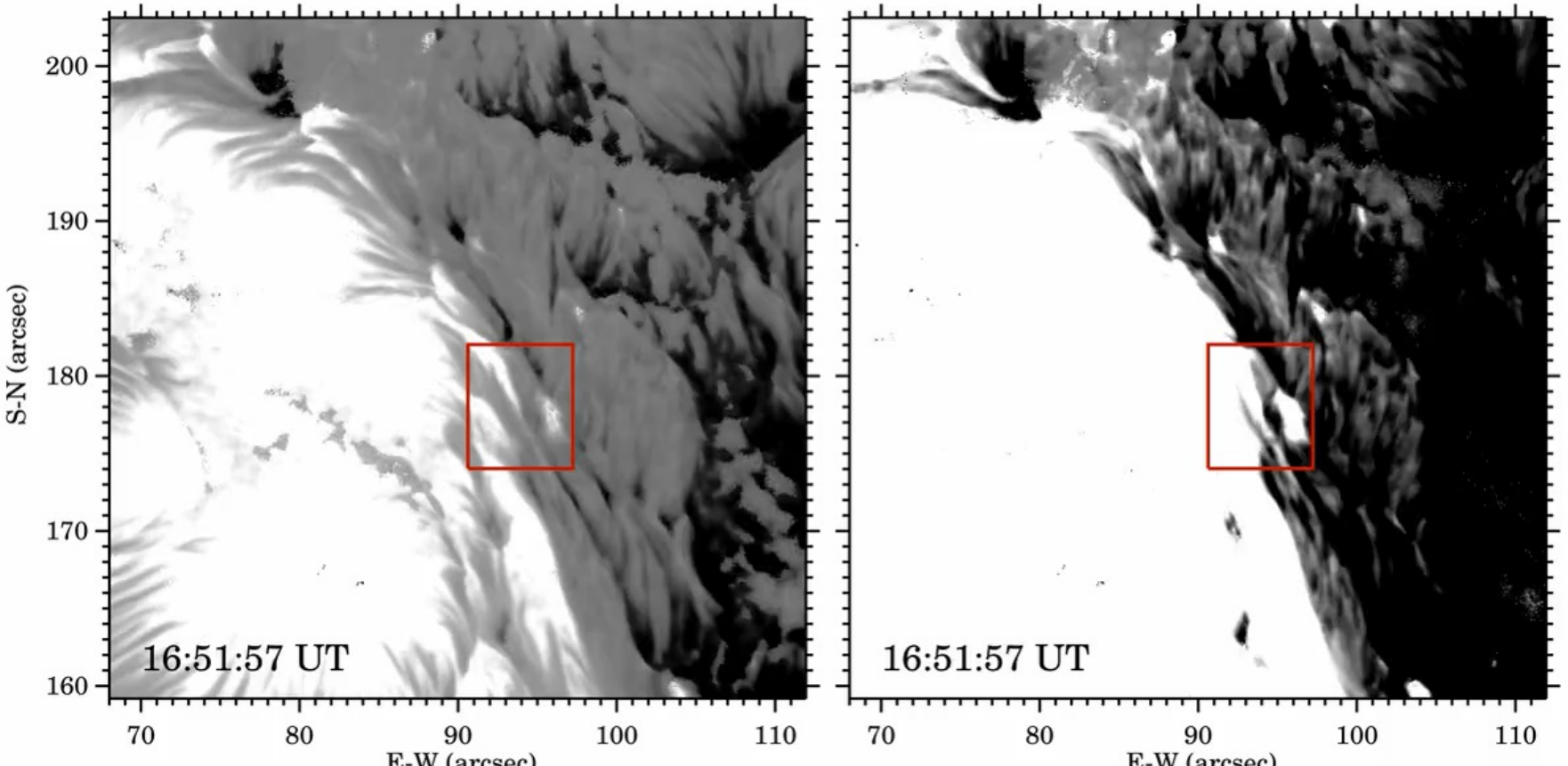

Microwave observations show that the emissions come from high B field areas first

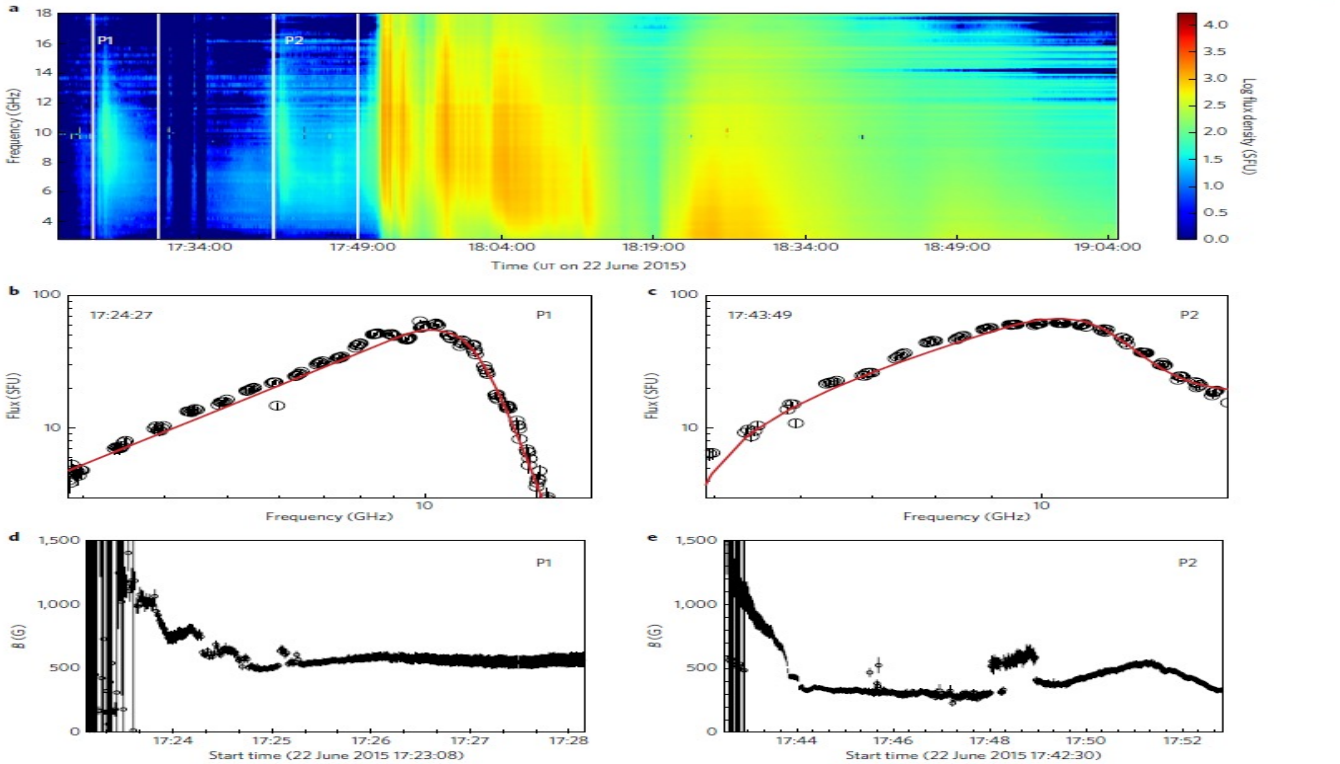

Very Unusual AR 12673, many studies on Sept. 6, 2017 X8.3 flare

- Shear Flow and Sunspot Rotation---Romano et al., 2018, Ap.JL, 852, L10, Verma, 2018, ApJ, in press; Yan et al., 2018, Ap.J. in press,
- Strong flux emergence—Sun and Norton, 2017, RNAAS, 1, 24
- Interaction between new flux and existing spot: Yang et al., 2017, Ap.JL, 849, L21
- MHD Modeling, Jaing et al. 2018, Nature Comm. Under review
- Strong Transverse Fields (>5000G), Wang et al., 2018, RNAAS, 2, 8
- Weak SEP event, largest WL emission, 2018, RNAAS, 2,7

Figure 1 from Strong Transverse Photosphere Magnetic Fields and Twist in Light Bridge Dividing Delta Sunspot of Active Region 12673
Haimin Wang et al. 2018 Res. Notes AAS 2 8 doi:10.3847/2515-5172/aaa670

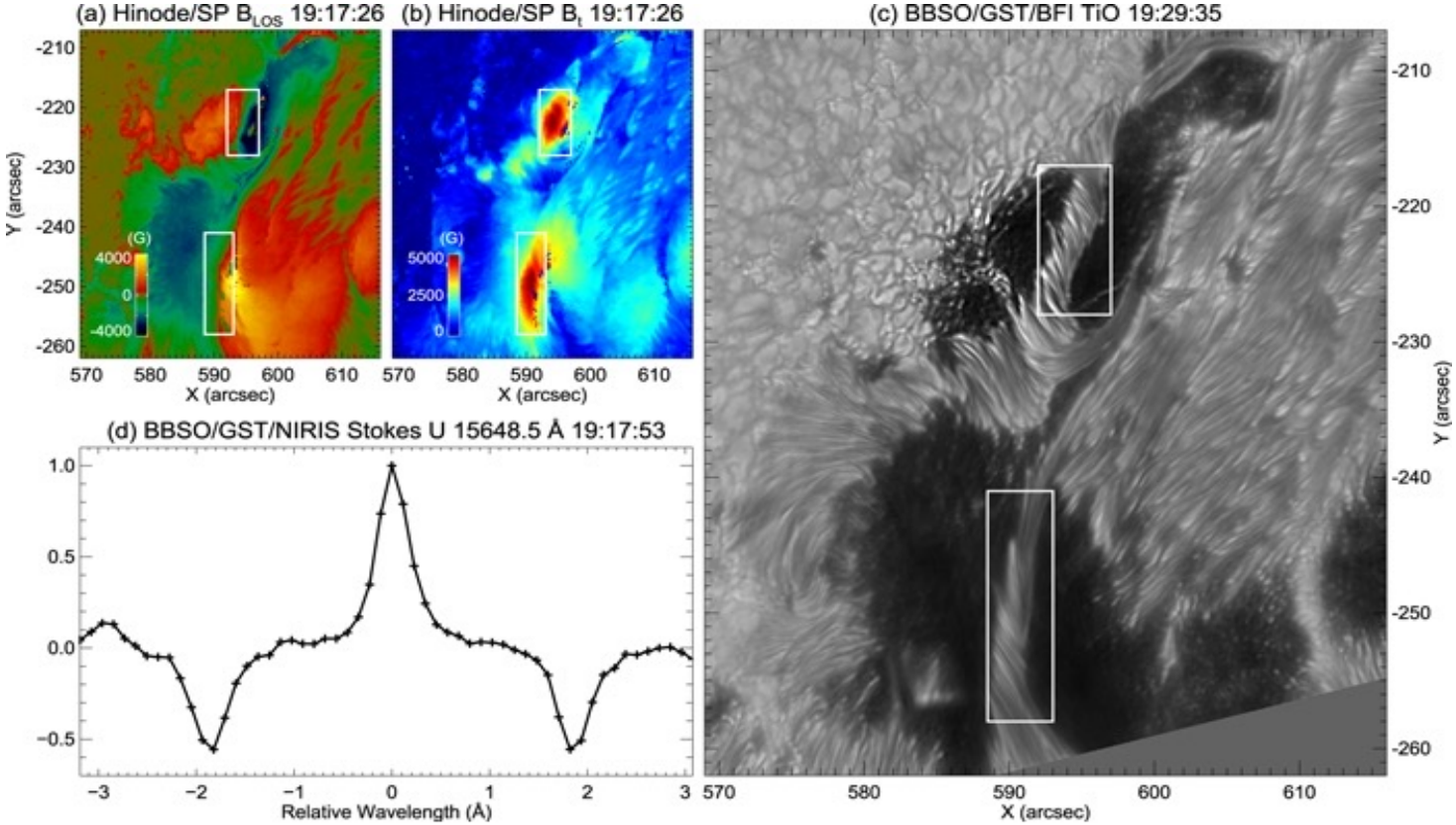

Negative Flare in He 10830

Xu et al., 2016, Ap.J, 819, 89

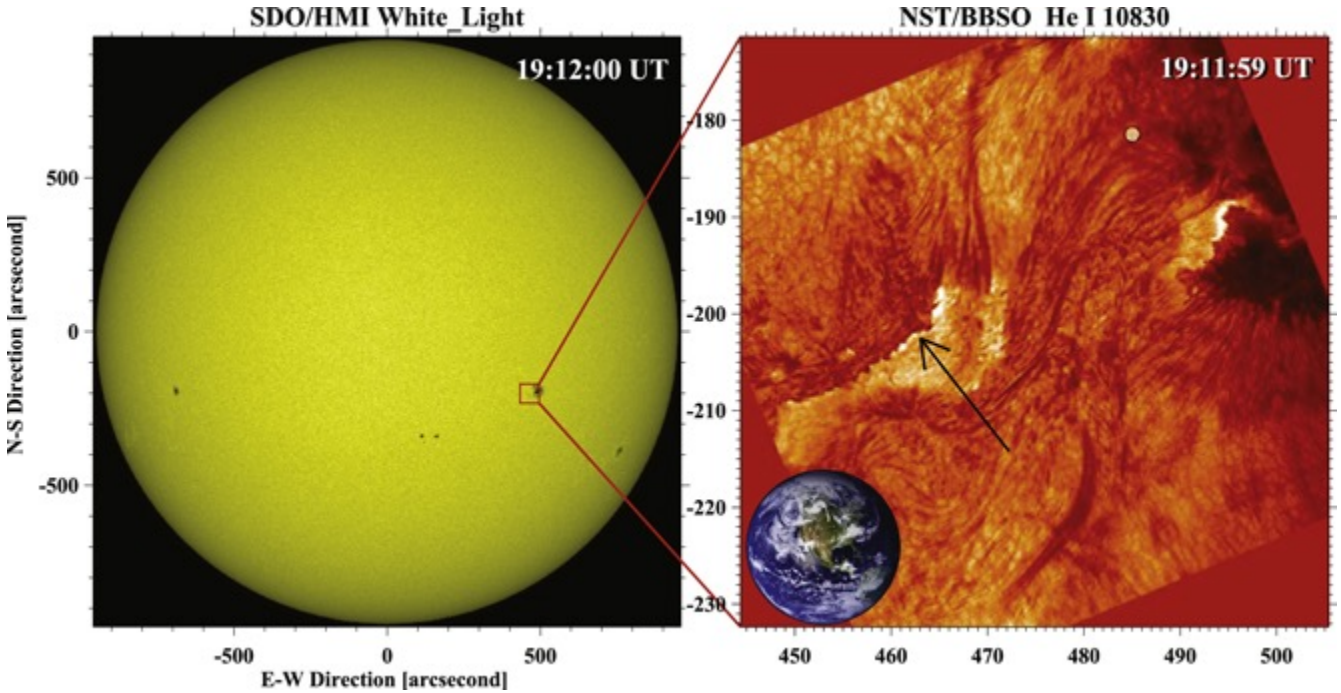

10830 Å Negative Flare observed by GST

2013-August-17

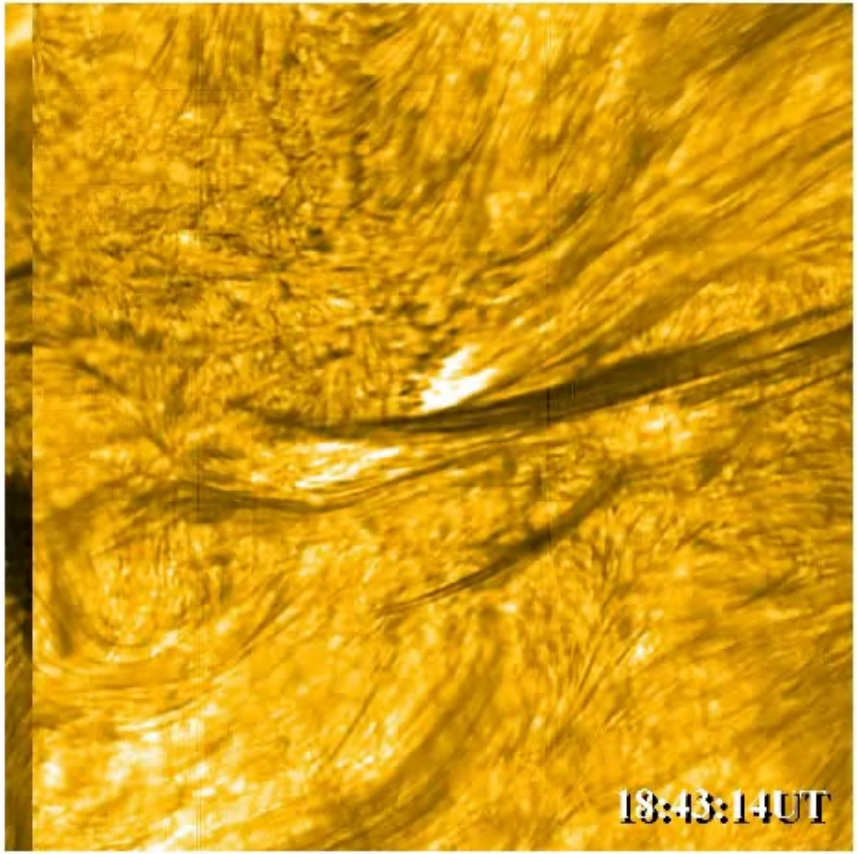

2013-August-17

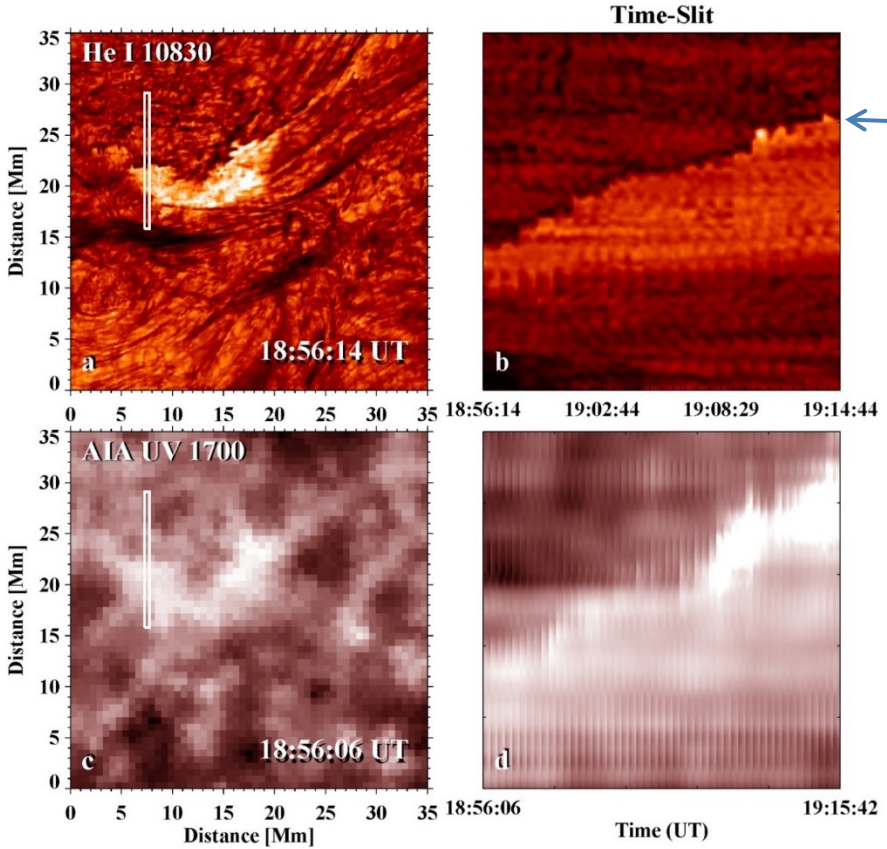

300 ~ 500 km

Impulse time of dimming 100 second

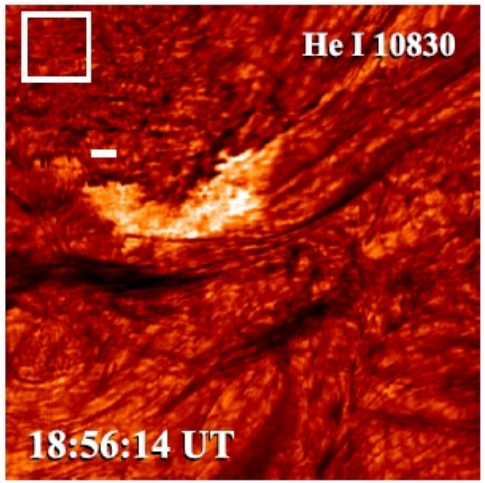

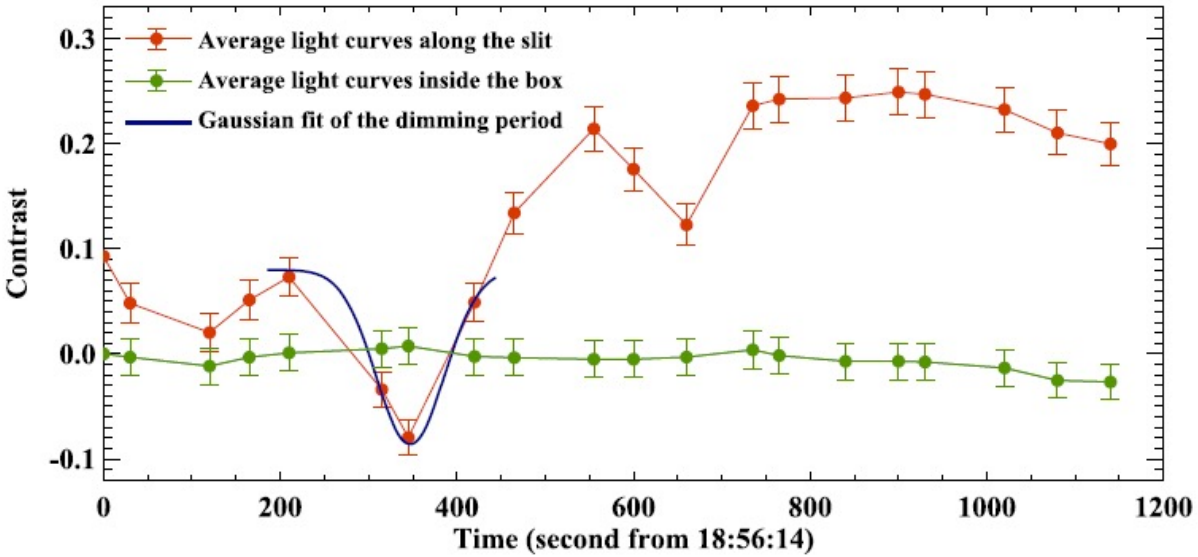

GST study of Flare Morphology and Magnetic Reconnection Rate (Cannon+ 2023)

The coronal magnetic reconnection rate, or reconnection flux per unit time in the standard 2D model (Forbes & Priest 1984): $\dot{\Phi} = \frac{\partial \Phi}{\partial t} = \frac{\partial}{\partial t} \int B da$

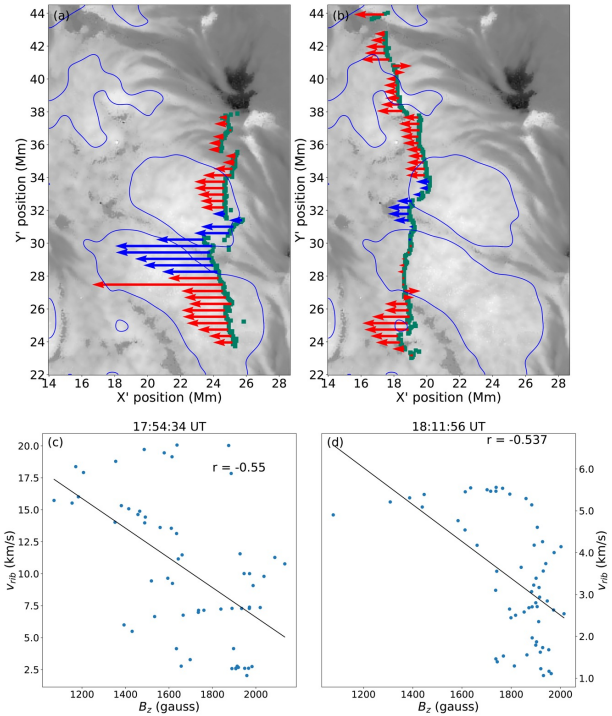

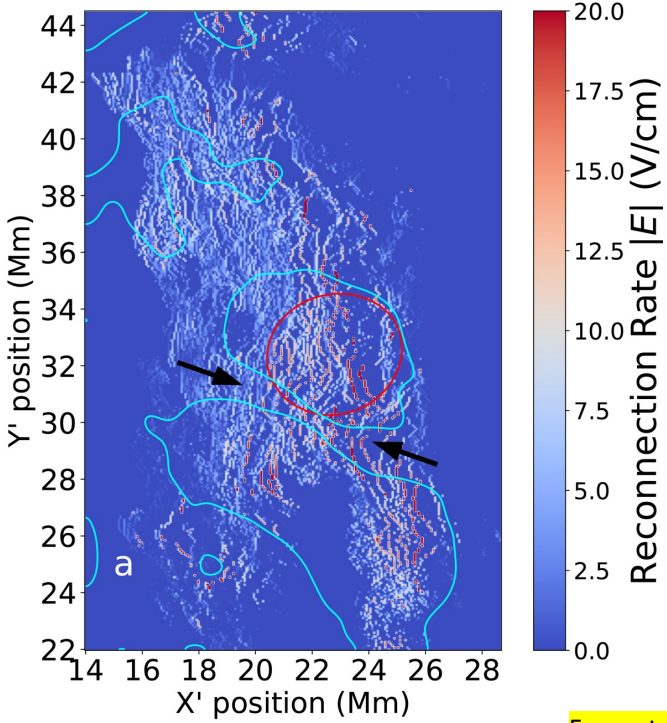

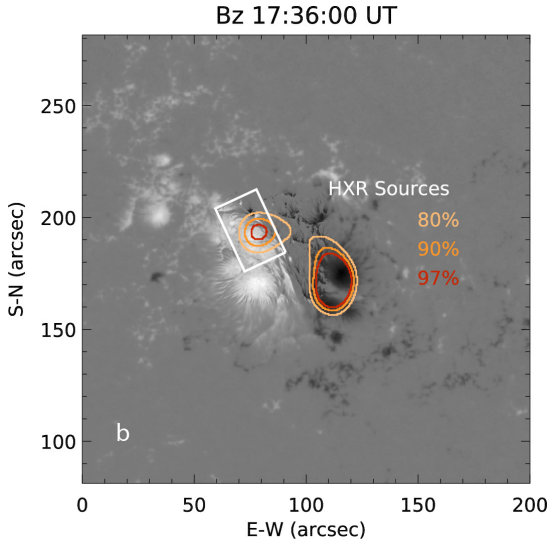

HMI B_LOS with NIRIS embedded, the RHESSI intensities (contours), and the FOV of the left panel (box).

Spatial distribution of reconnection rate, E, RHESSI HXR intensity (red contour of 97% of maximum) and 48% maximum of the smoothed GST Ha intensity (blue contours) outline the sunspots. Two ends of the LB (arrows).

- For certain times and locations, the large velocity coincides with weak magnetic field.
- Around the LBs, the velocity and current density are enhanced.

Coronal Magnetic Field Extrapolation and Topological Analysis of Fine-scale Structures during Solar Flare Precursors

He, Wen (DKIST Ambassador) et al., 2023, ApJ 958, 90

BBSO NIRIS data is embedded in HMI data to extrapolate coronal magnetic field

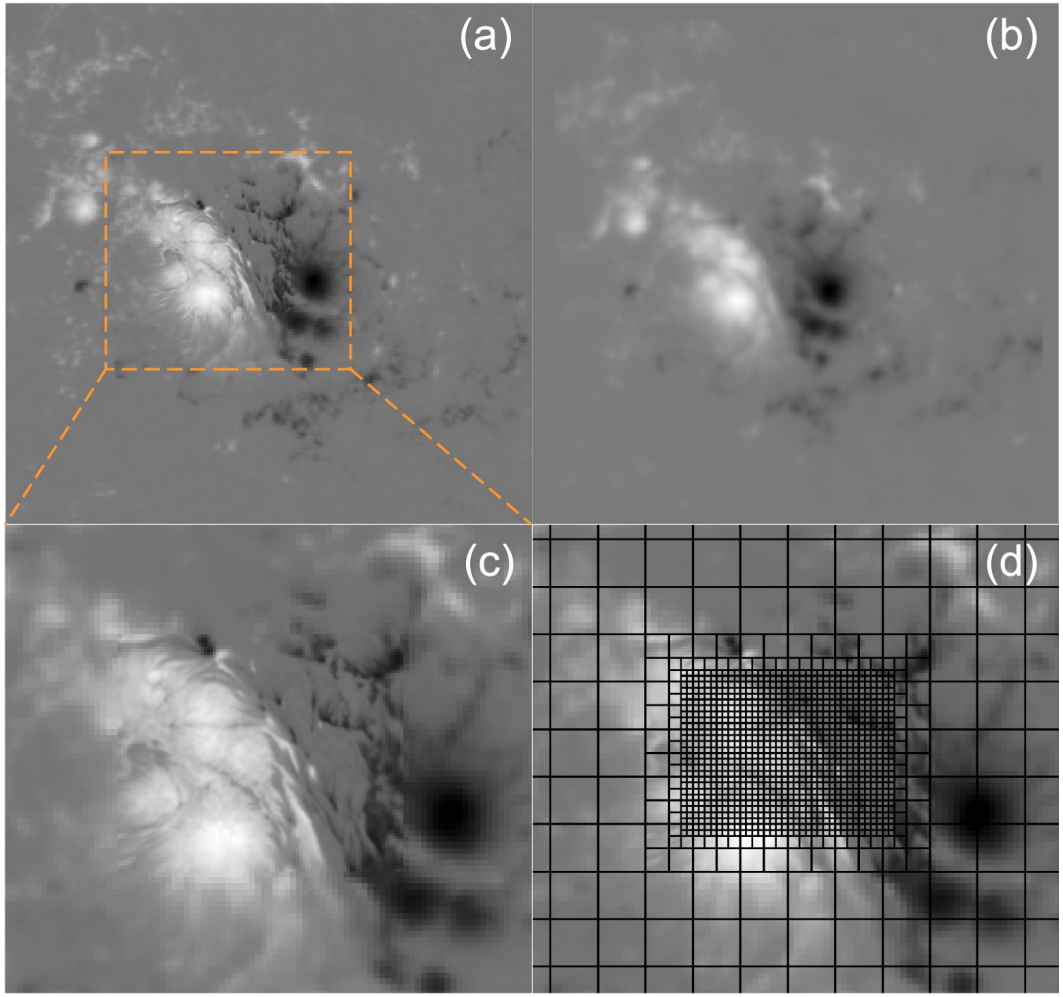
(a)
(b)
(c)
(d)

Extrapolations showing low-lying fluxropes

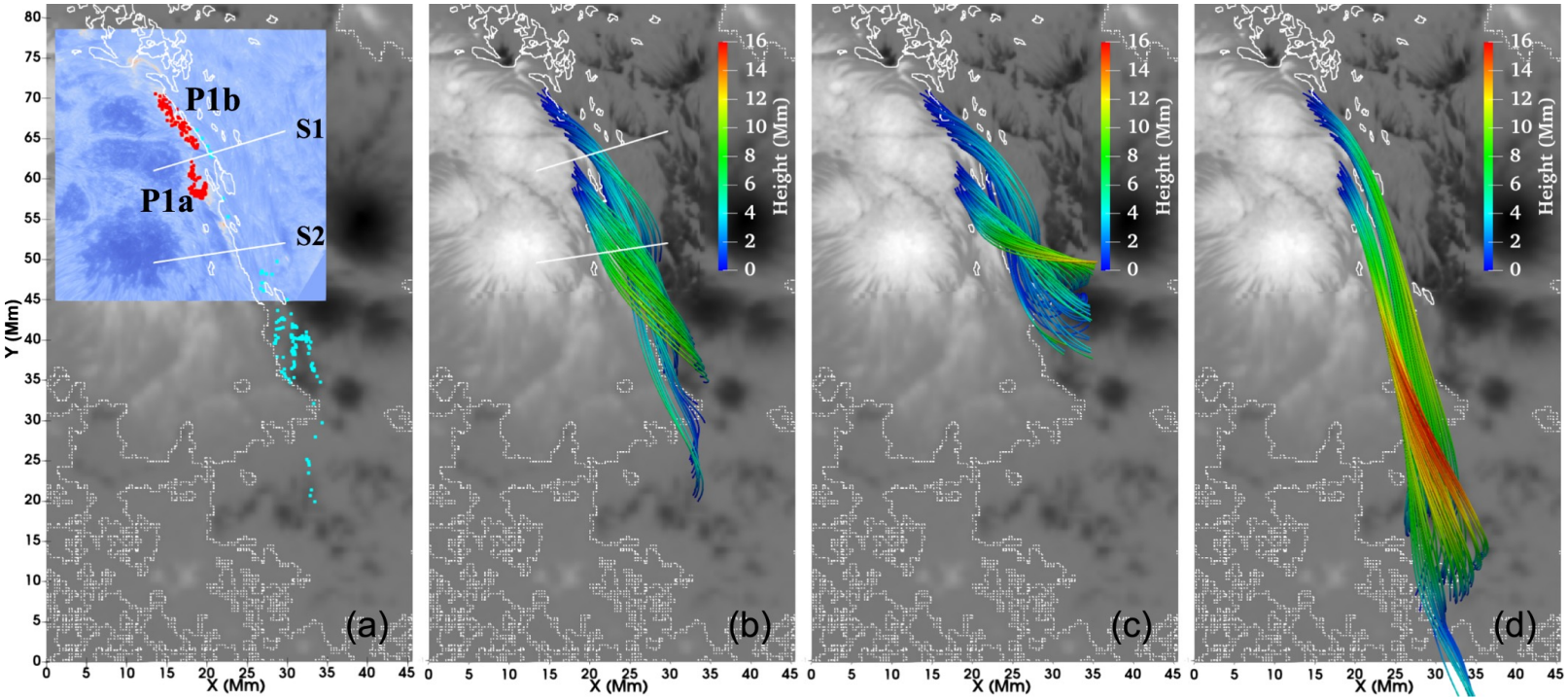

Key Findings

For all three extrapolation runs, the field line connectivity around the precursor brightenings is compared with the GST/Hα observations. The magnetic field lines originating from the precursor brightening regions exhibit a configuration of the fine-scale magnetic structures beyond the small FOV of GST, but are confined within the larger FOV of HMI, more consistent with the spatial extent of the main PIL between two main magnetic polarities. Multiple sheared flux bundles are found to overlie across the main PIL, with groups of footpoints rooted in the positive magnetic polarity regions and coinciding with each set of the observed Hα brightening patches.

Solar Flares Triggered by a Filament Peeling Process Revealed by High-resolution GST Ha Observations

Mia Mancuso (DKIST Ambassador), Ju Jing, Haimin Wang, and Wenda Cao

BBSO, NJIT

NJIT

NSF

Data & Observations: The Event

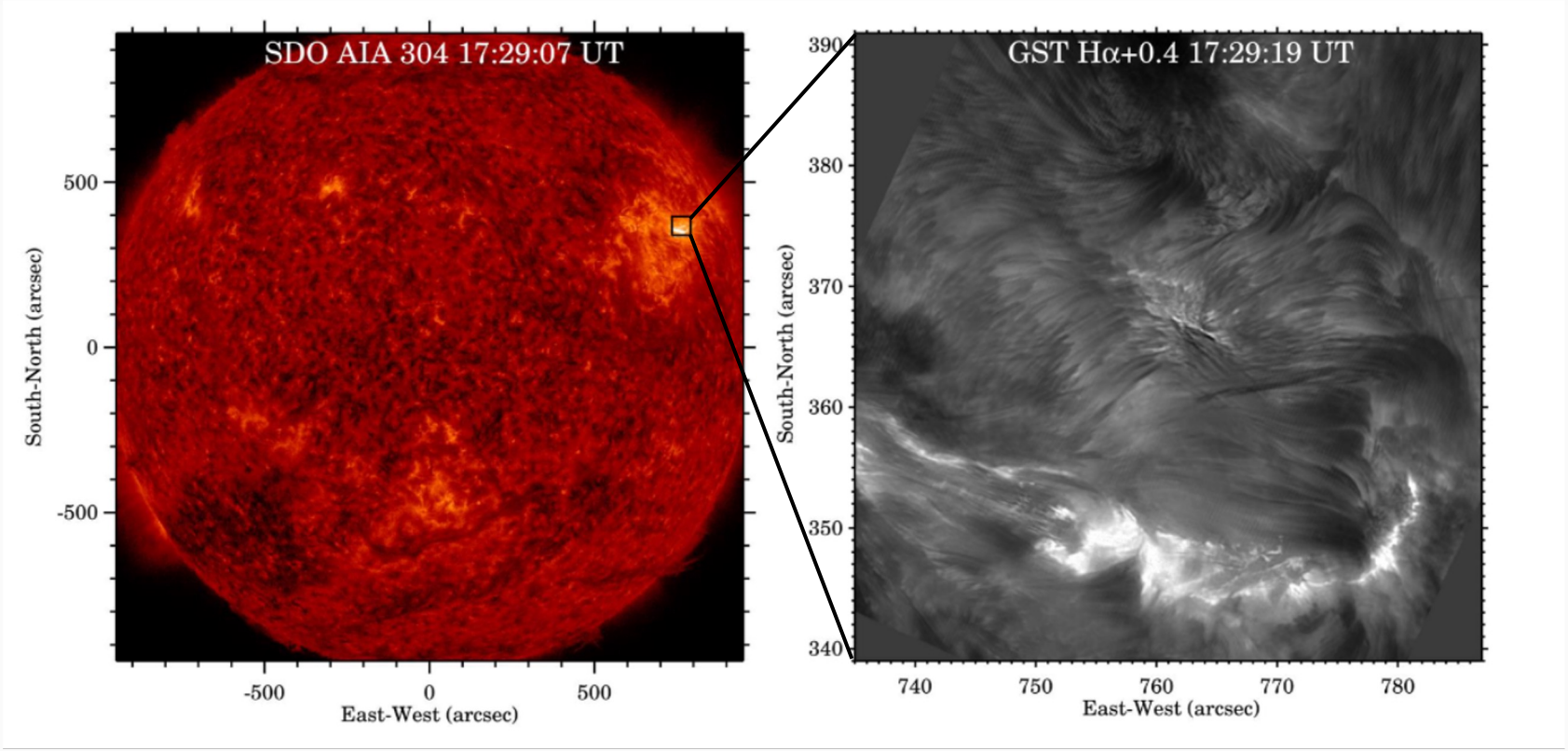

Two successive C-class solar flares, C5.4 (SOL2022-11- 14T17:24) and C5.1 (SOL2022-11-14T19:29), from the same active region: NOAA active region 13140 on Nov. 14, 2022.

Data & Observations: Concurrent CME

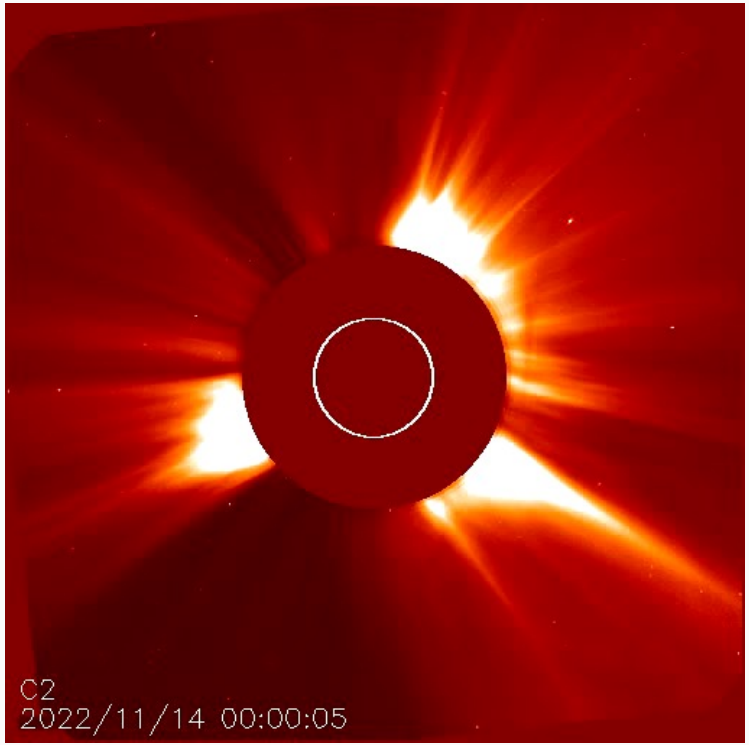

LASCO C2 observation of the CME. The CME is concurrent in time and location with the flares observed in Hα. It is the second one to appear in this video.

Data & Observations : Hα Observation

GST Hα +0.4 Observation:

- Three brightening but only two flares
- Filament movement prior to eruption
- Only small portion of filament erupts
- Overall structure consistent

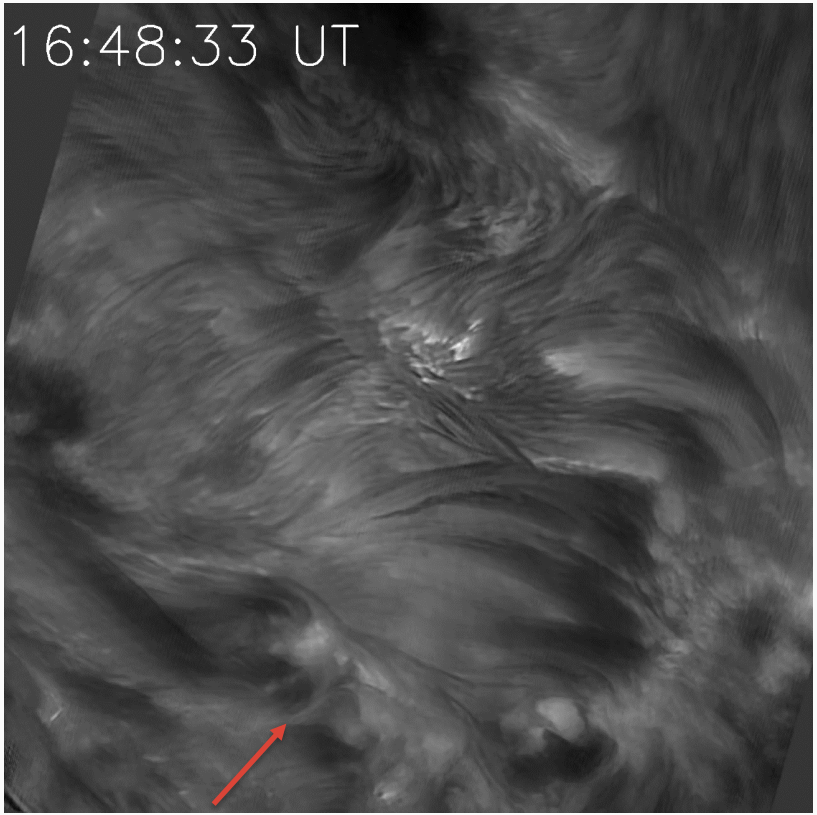

Results: Time-Distance Analysis

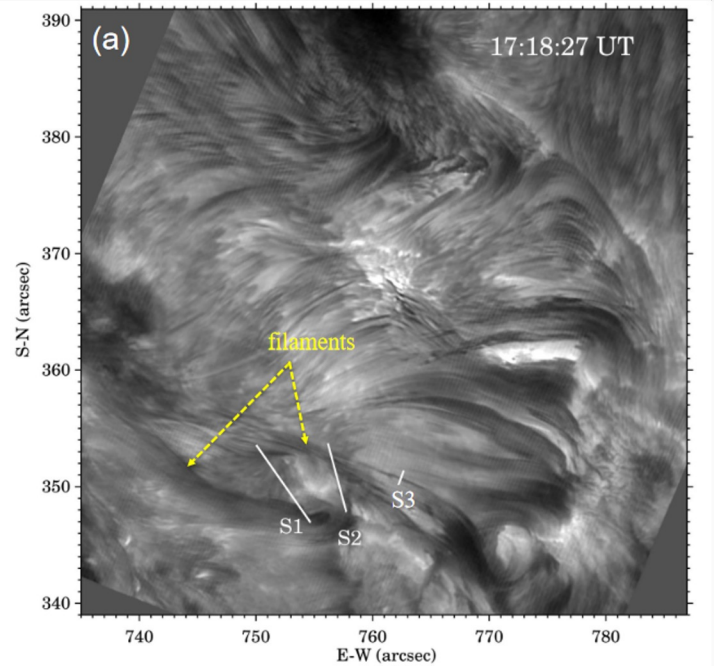

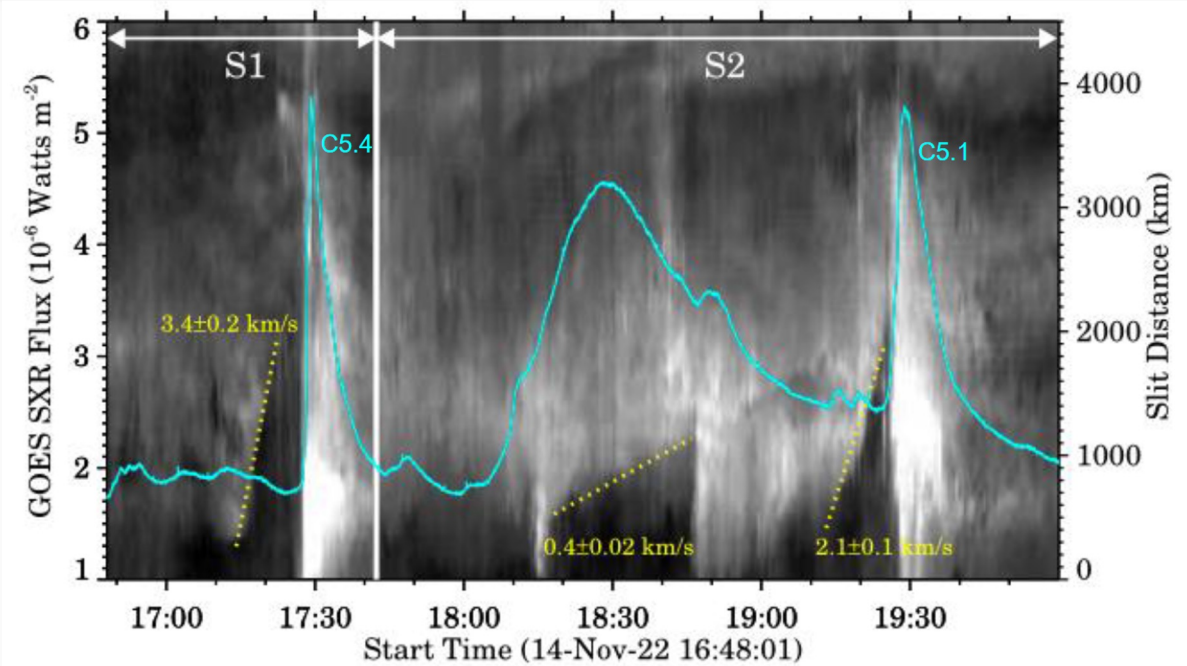

Slits S1 and S2 used to for the creating the time distance plot for the first and second flare respectively. S3 gives the approximate size of a peeling strand (~168km)

Time distance plot with GOES SXR flux overplotted in cyan, yellow dashed lines represent the approximate velocities of the filament motion.

Smallest two ribbon flare associated with mini-filament eruption (Wang, J., et al., 2024, ApJ, under review). They may be numerous, contributing coronal heating and solar wind structures such as switchbacks and small scale fluxropes.

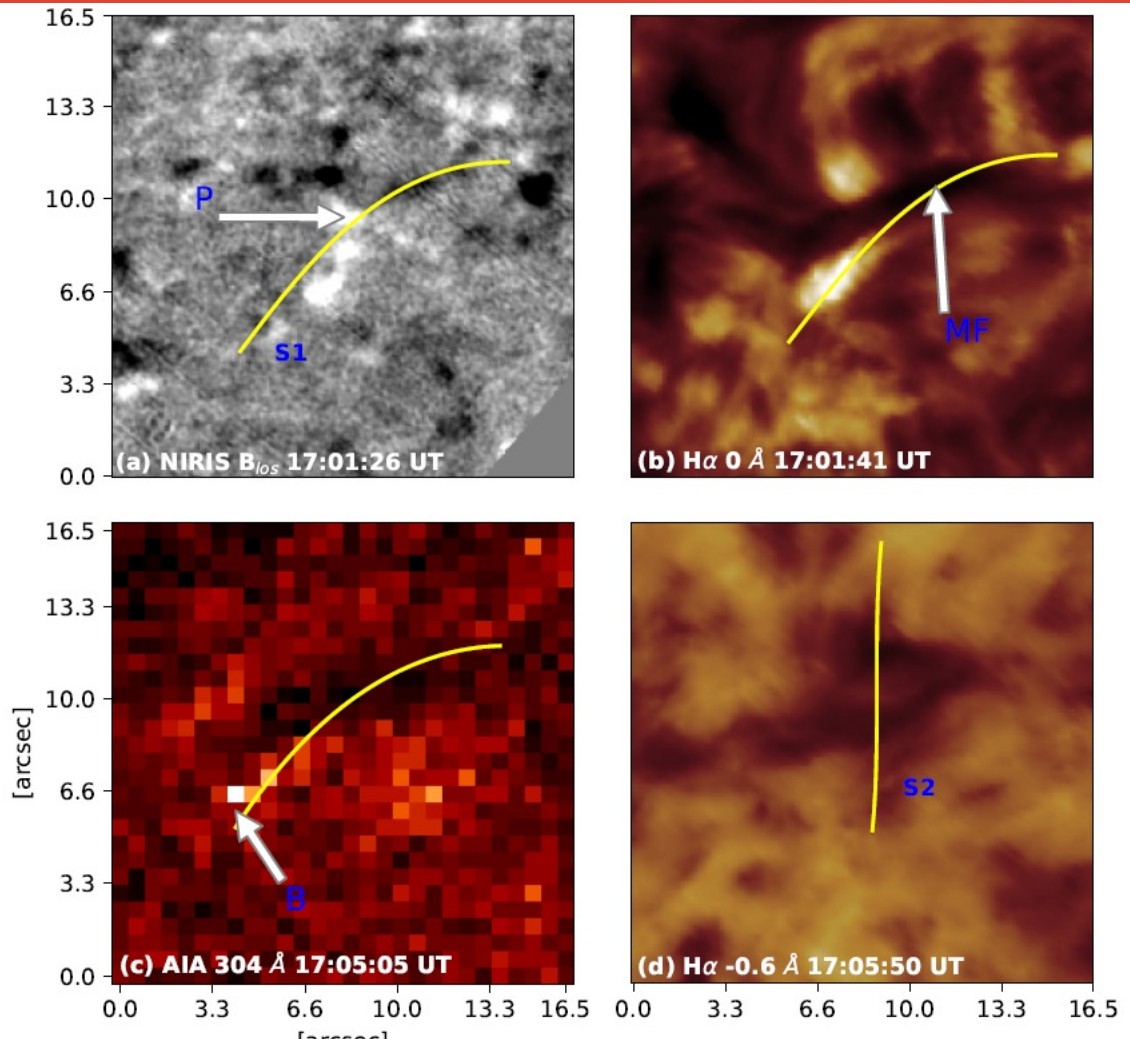

BBSO/GST Observations of Minifilament activities

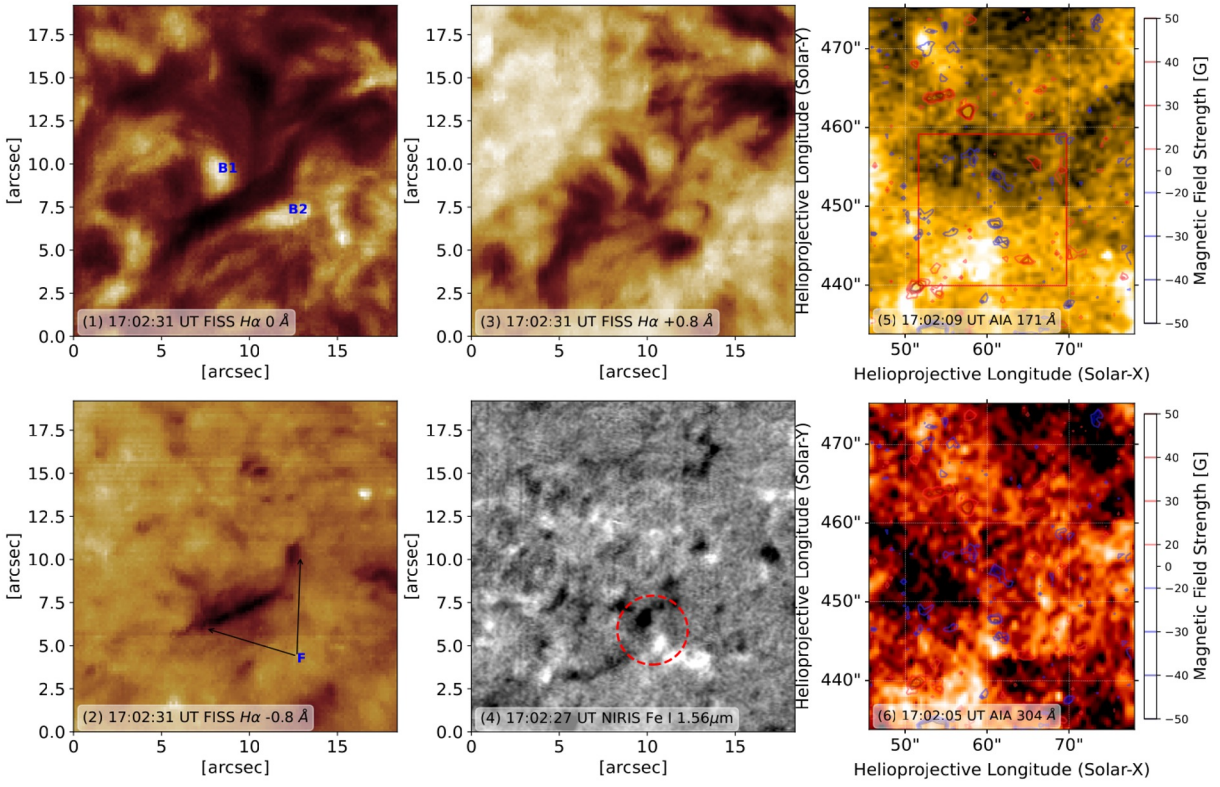

- Fast Imaging Solar Spectrograph (FISS): Four dimensional spectra simultaneously recorded in Hα(6563Å) and the Ca II(8542Å) band, with 0.16'' resolution and 25 s cadence.
- Near Infrared Imaging Spectropolarimeter (NIRIS): magnetogram in 1.56 μm, with 0.2" resolution and 62 s cadence.

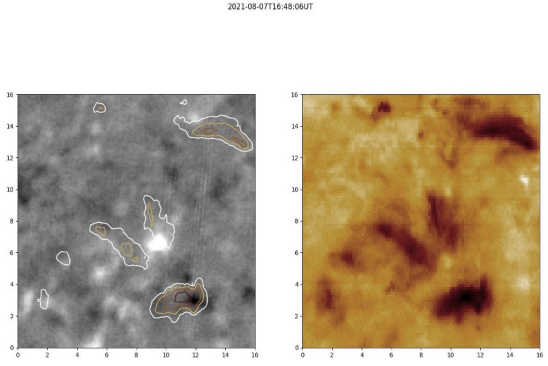

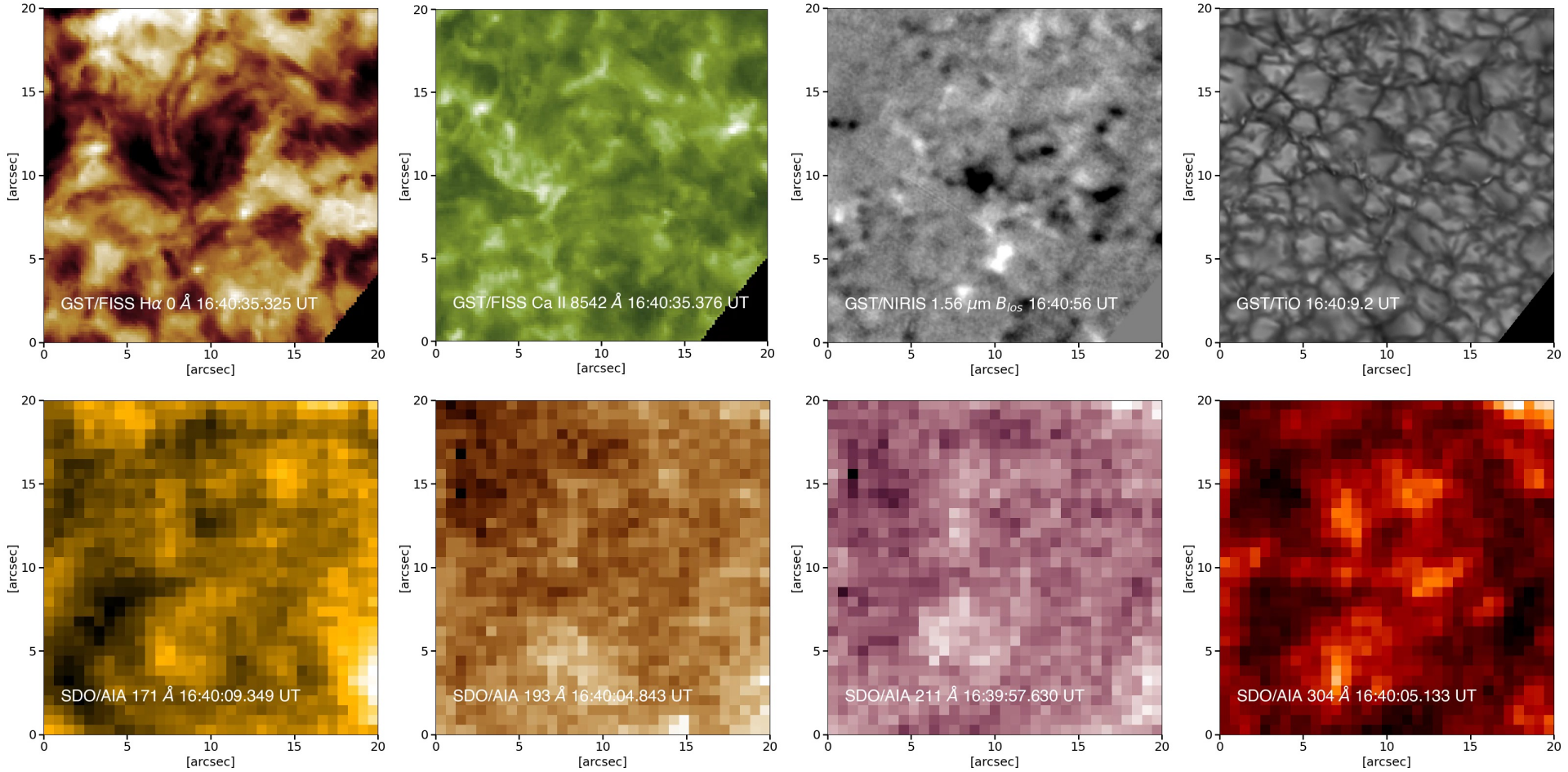
GST/FISS Hα 0 Å 16:40:35.325 UT
GST/FISS Ca II 8542 Å 16:40:35.376 UT
GST/NIRIS 1.56 μm B_{los} 16:40:56 UT
GST/TiO 16:40:9.2 UT
SDO/AIA 171 Å 16:40:09.349 UT
SDO/AIA 193 Å 16:40:04.843 UT
SDO/AIA 211 Å 16:39:57.630 UT
SDO/AIA 304 Å 16:40:05.133 UT
[arcsec]
0
5
10
15
20

FISS Spectral Inversion Results

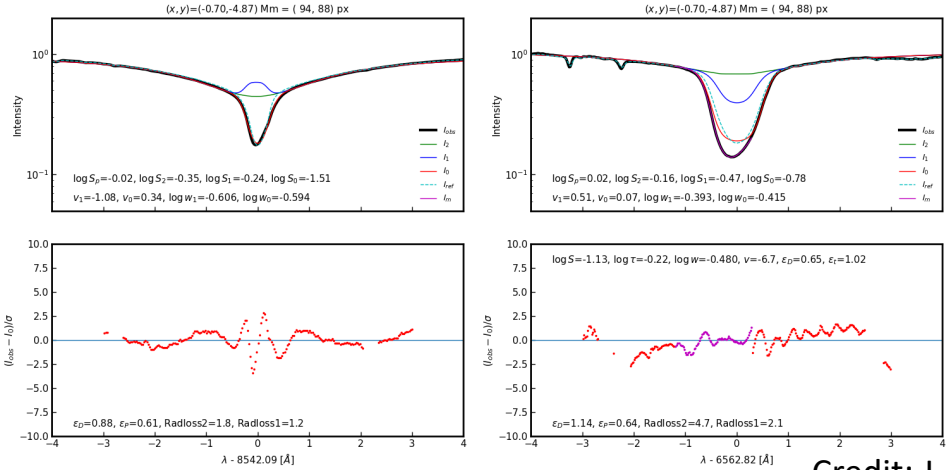

Credit: J. Chae

The Hα profile fitting is based on the 4-layer model fit of the profile. The top layer is like a cloud. The wavelengths in the cloud range [-1.2 A, 0.30A] has been fitted by the 4-layer model, while those outside, by 3-layer model.
The filament is characterized by source function of 10^-1.13, optical depth of 10^-0.22, Doppler width of 10^-0.48 A, and Doppler velocity of -6.7 km/s.
The Doppler width of the H alpha in combination with the Ca II Doppler width of 10^-0.6 A yields the temperature estimate of 9400 K.

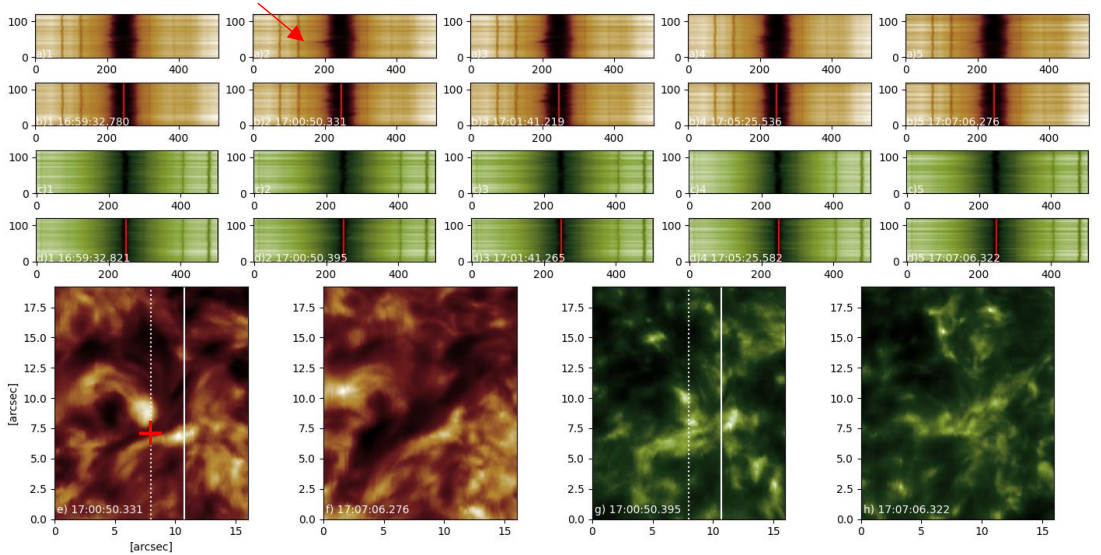

High Cadence Observations of Flares—Towards the understanding of elementary bursts (Yan Xu)

North Ribbon

Red wing

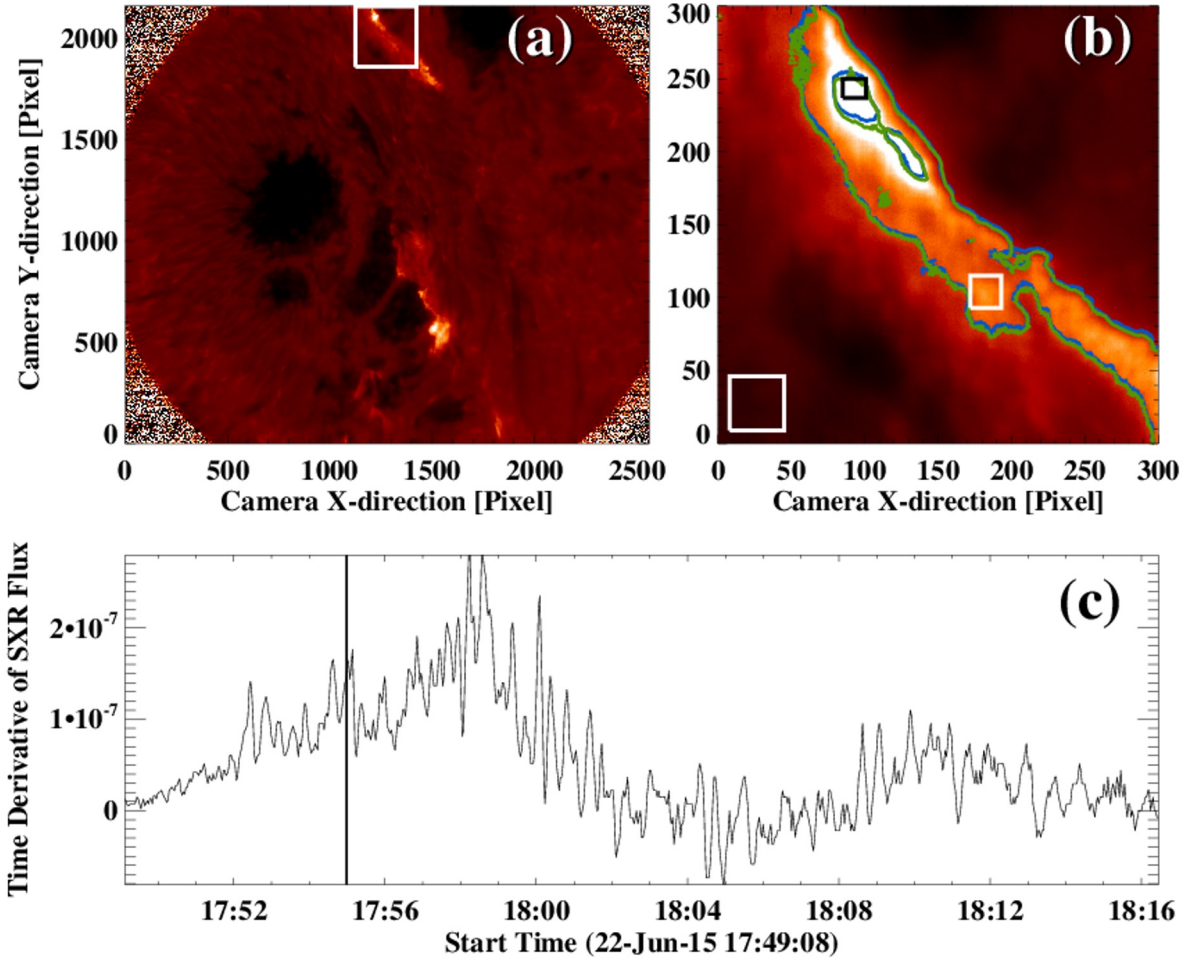

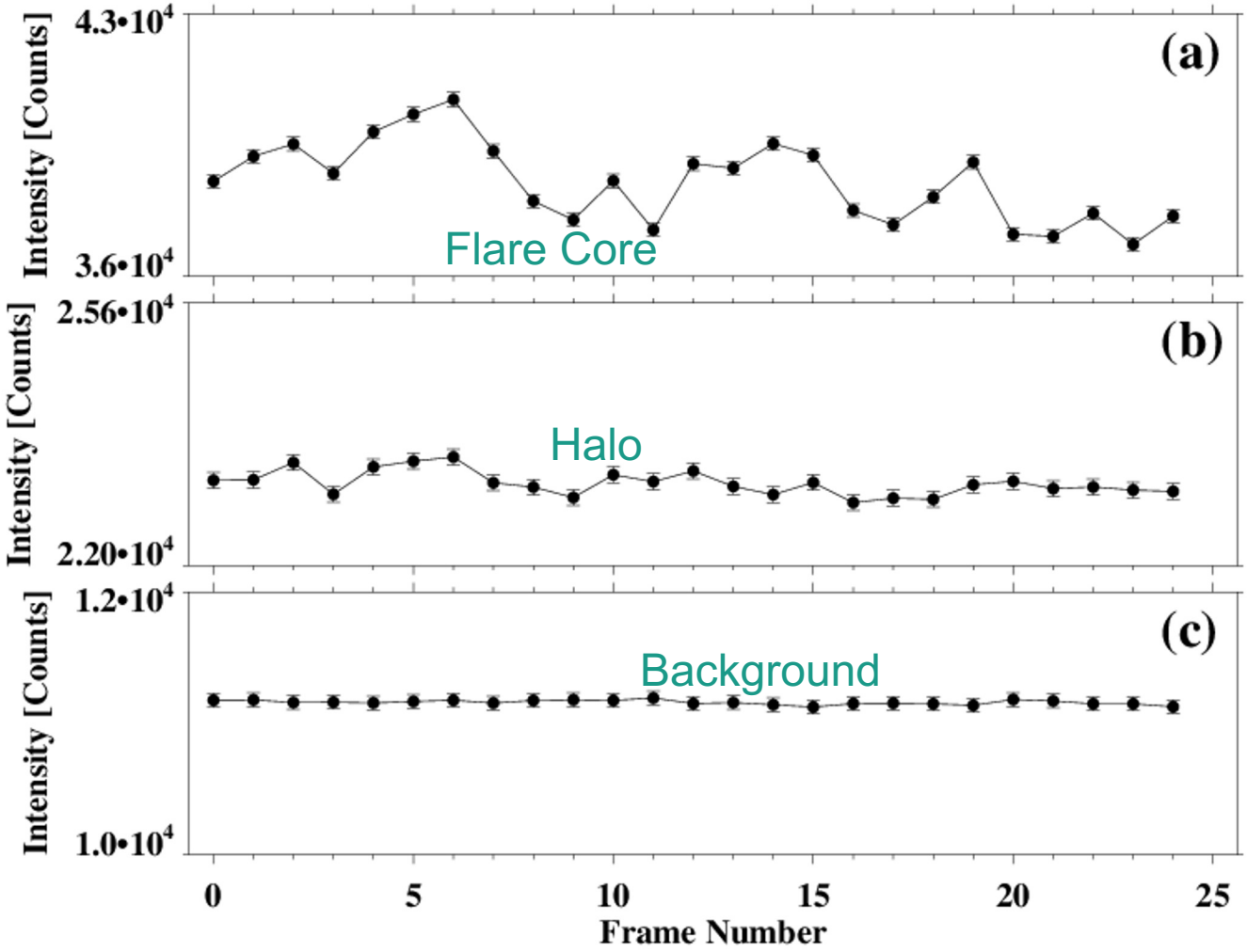
(a)
Flare Core
Intensity [Counts]
4.3•10^4
3.6•10^4
(b)
Halo
Intensity [Counts]
2.56•10^4
2.20•10^4
(c)
Background
Intensity [Counts]
1.2•10^4
1.0•10^4
0
5
10
15
20
25
Frame Number

Concluding Remarks

- BBSO/GST provides a unique tool in study solar atmosphere and activities due to excellent seeing conditions covering several hours a day. GST and DKIST are highly complementary. GST is especially important for flare observations.
- Flare ribbon fronts, pre- and post-flare loops are in the scale of about 100 km. The injection flare electron flux should increase substantially comparing to the results from RHESSI (2" resolution).
- In He10830, flare front may appear as narrow dark front, indicating the effect of collisional ionization.
- Irreversible/rapid photospheric magnetic structures are detected such as formation of new penumbra, rapid sunspot rotation and sudden transvers field orientation change.
- Partial eruptions of filaments may explain repeated flaring, small amount of fluxes may be separated from larger fluxrope due to internal reconnection.